RSC Advances

This article can be cited before page numbers have been issued, to do this please use: A. Guarnizo, I. Angurell, G. Muller, J. Llorca, M. Seco, O. Rossell and M. Rossell, *RSC Adv.*, 2016, DOI: 10.1039/C6RA14257E.

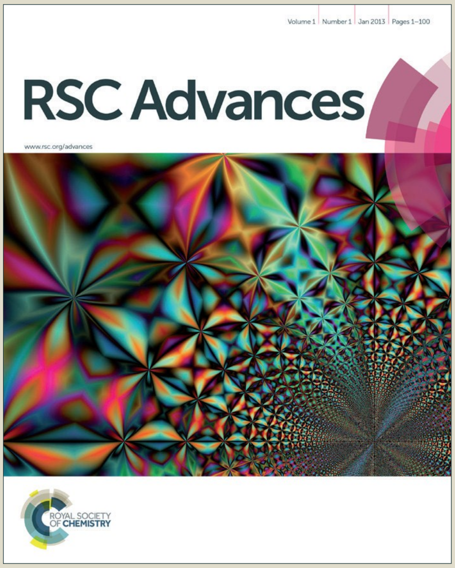

ROYAL SOCIETY OF CHEMISTRY

www.rsc.org/advances

ROYAL SOCIETY OF CHEMISTRY
View Article Online
DOI: 10.1039/C6RA14257E

Journal Name

ARTICLE

Received 00th January 20xx,
Accepted 00th January 20xx

DOI: 10.1039/x0xx00000x

www.rsc.org/

Highly water-dispersible Pd nanoparticles and single atoms magnetite-supported as excellent catalysts for Suzuki and hydrogenation reactions

A. Guarnizo,[a] I. Angurell,*[a] G. Muller,[a] J. Llorca,[b] M. Seco,[a] O. Rossell,[a] and M. D. Rossell*[c]

The molecule 4-(diphenylphosphino)benzoic acid (dpa) anchored on the surface of magnetite nanoparticles permits the easy capture of palladium ions that are deposited on the surface of the magnetite nanoparticle after reduction with $NaBH_4$. Unexpectedly, a significant fraction of dpa is removed in this process. Samples of Fe_3O_4dpa@Pd_x containing different Pd loading (x= 0.1, 0.3, 0.5 and 1.0 wt%) were prepared and their catalytic efficiency for the Suzuki C-C coupling reaction studied. The best catalyst was Fe_3O_4dpa@$Pd_{0.5}$ that gave the highest TOF published up to now for the reaction of bromobenzene with phenylboronic acid in a mixture of ethanol/water (1/1). Interestingly, the same reaction carried out in water produced also excellent yields of the resulting C-C coupling product. The behaviour of other bromide aryl molecules was also investigated. The best catalytic results for the aqueous phase reduction of 4-nitrophenol (4-NP) to 4-aminophenol (4-AP) were obtained using Fe_3O_4dpa@$Pd_{0.1}$. The presence of Pd SACs (single atom catalyst) seems to be responsible for this performance. In contrast, the same Fe_3O_4dpa@$Pd_{0.1}$ catalyst is absolutely inactive in the hydrogenation of styrene in ethanol.

Introduction

For the last few decades Pd nanoparticles (NPs) have attracted enormous attention as transition metal catalyst in the array of transformation processes in organic chemistry, mainly for C-C cross-coupling reactions.[1] Given that easy aggregation of nanoparticles can affect their catalytic behaviour it is crucial to protect them with appropriate linkers, namely, thiol-protected linkers,[2,3] dendrimers,[4] dendrons[5] or by the use of ionic liquids.[6] Other strategy involves the immobilization of the Pd NPs on solid supports, usually SiO_2, TiO_2 and C prepared by different procedures and having different areas and morphologies.[7] This interest has increased in the last years with the easy deposition of Pd onto the surface of magnetite NPs allowing to obtain catalytic systems magnetically separable that avoid the requirement of catalyst filtration after completion of the reaction. In addition, the nanocatalyst can be efficiently recycled and reused in the vast majority of examples.[8] For anchoring small and homogeneous nanoparticles it is worth functionalizing previously the magnetite surface with linkers terminated generally with amino[9,10] or phosphine units.[11] However, the benefits produced by the linkers on the deposition of the metal catalysts should be contrasted with the potential catalytic inhibition produced by their steric hindrance that difficults the approach of the reagents to the catalyst. In this context, it is evident that the possibility of partial removal of the linker after metal immobilization becomes a desirable condition.

Very recently, we have reported the synthesis and use of 4-mercaptophenyldiphenylphosphine (Sdp) as linker to immobilize Pd nanoparticles onto the surface of magnetite nanoparticles.[12] Subsequent treatment of the nanoparticles with an aqueous hydrogen peroxide solution permitted the removal of 70wt% of Sdp. The partial loss of the linker made the resulting nanoparticles catalytically more efficient for Suzuki-Miyaura C-C cross coupling reaction and for hydrogenation of 4-nitrophenol and styrene.

In this paper we expand this study to the formation of Pd/magnetite nanoparticles and single-atoms using the partially water soluble and commercially available 4-(diphenylphosphino)benzoic acid (Fig. 1) as a linker in order to make the above processes "greener" by minimizing the use of (toxic) organic solvents. In addition to this, the increased demand for scare metals as palladium and future availability[13] is a matter for concern that would be dispelled if a control of the palladium particle size is achieved for proper atomic economy.

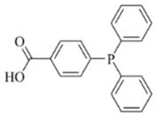

Fig. 1 4-(diphenylphosphino)benzoic acid (dpa)

---

[a] Departament de Química Inorgànica i Orgànica, Secció de Química Inorgànica, Universitat de Barcelona, Martí i Franquès 1-11, 08028 Barcelona (Spain). e-mail: inmaculada.angurell@qi.ub.es.
[b] Institut de Tècniques Energètiques i Centre de Recerca en Nanoenginyeria, Universitat Politècnica de Catalunya, Diagonal 647, 08028 Barcelona (Spain).
[c] Electron Microscopy Center, Empa, Swiss Federal Laboratories for Materials Science and Technology, Überlandstrasse 129, 8600 Dübendorf (Switzerland). e-mail: marta.rossell@empa.ch.

†Electronic Supplementary Information (ESI) available: XPS of catalysts (Fig. S1), tables of conversion in Suzuki-Miyaura based on temperature (in ethanol/water) (Table S1), base (Table S2), solvent (Table S3) and temperature in water solution (Table S4). See DOI: 10.1039/x0xx00000x

View Article Online
DOI: 10.1039/C6RA14257E

Results and discussion

Synthesis of the catalysts

The starting bare magnetite nanoparticles were synthesized following a literature procedure.[14] Functionalized magnetite nanoparticles Fe_3O_4dpa were obtained by sonication of Fe_3O_4 in methanol in presence of dpa during 2 hours (Scheme 1a). Elemental analyses (C, H) of the resulting nanoparticles showed that the load of the organic component was about 3.2 wt%. The next step consisted of immobilizing Pd onto the magnetite surface (Scheme 1b). Thus, Fe_3O_4dpa was dispersed in water and sonicated for 10 min. Then, a water solution of $K_2[PdCl_4]$ followed by another of sodium borohydride were added to obtain the Fe_3O_4dpa@Pd_x nanoparticles where x is the weight Pd percentage in the NPs. With this method, we prepared several samples with different Pd contents (0.1%, 0.3%, 0.5% and 1.0%). The first one was included in order to obtain magnetite NPs decorated exclusively with isolated palladium single atoms. These species are denoted as SACs (single-atom catalyst)[15] and exhibit generally exceptional catalytic activity.

A crucial and surprising observation in the course of the Fe_3O_4dpa@Pd_x NPs fabrication was the significant fraction of dpa lost during the reduction process with $NaBH_4$. For example, the Fe_3O_4dpa@$Pd_{0.5}$ only kept 1.7% dpa from 3.2% of the starting Fe_3O_4dpa NPs. That is, dpa favours the dispersion of Pd NPs on the magnetite surface and then the ligand undergoes partial elimination without the need of using other agents. Consequently, the poor linker content in Fe_3O_4dpa@Pd_x NPs anticipated excellent catalytic activity that we have explored in the Suzuki-Miyaura reaction, reduction of 4-nitrophenol and styrene hydrogenation processes.

Characterization of Fe_3O_4dpa@Pd_x NPs. The FT-IR spectrum of the catalysts are practically identical showing a sharp peak at 594 cm^{-1}, which is the IR signature for ferrite particles and weak signals at 1100 cm^{-1} and 2921 cm^{-1} (fig. S1) due to aryl C-H vibrations. The Pd content in Fe_3O_4dpa@Pd_x was determined by ICPoes (Inductive Coupled Plasma optical emission spectroscopy) measurements and the dpa content was estimated by OEA (Organic Elemental Analysis). The analytical composition of the hybrids, as well as of the NPs loaded with Pd in the absence of linker, is shown in Table 1.

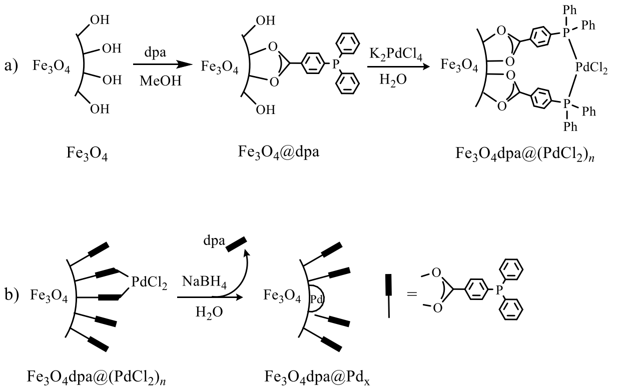

Scheme 1 Synthesis of catalysts: (a) MNPs functionalization with dpa and Pd(II) capture and (b) deposition of palladium nanoparticles and partial dpa lost.

Table 1 Composition of magnetite-dpa-Pd hybrids

Catalyst	% dpa (nmol/mg NPs)	%Pd
Fe_3O_4dpa	3.2 (105)	0
Fe_3O_4@Pd	0 (0)	0.68
Fe_3O_4dpa@$Pd_{0.1}$	2.4 (78.7)	0.097
Fe_3O_4dpa@$Pd_{0.3}$	1.9 (63.0)	0.32
Fe_3O_4dpa@$Pd_{0.5}$	1.7 (55.2)	0.51
Fe_3O_4dpa@$Pd_{1.0}$	1.1 (35.0)	1.01

Images of the hybrid nanoparticles Fe_3O_4dpa@Pd_x have been obtained by TEM (for x = 1.0) and HAADF-STEM (High-Angle Annular Dark-Field Scanning Transmission Electron Microscopy) (for x = 0.1, 0.3, and 0.5). The samples display spherical Fe_3O_4 nanoparticles with an average particle size around 12 nm. In addition, smaller Pd species appear immobilized on the magnetite surface. As expected, the total Pd load determines the Pd nanoparticle size. Thus, for x= 1.0 the images clearly reveal the presence of nanoparticles with an average size of 4.5 nm (Fig. 2). In contrast, when the Pd loading is 0.1 wt%, all Pd species exist exclusively as isolated single atoms; neither subnanometre clusters nor nanoparticles were detected at all (Fig. 3). Samples containing intermediate palladium contents, x = 0.3 and 0.5, evidenced numerous single metal atoms accompanied with other subnanometer clusters and larger nanoparticles. This fact is somewhat surprising because the presence of large nanoparticles of ~5 nm along with a significant number of Pd SACs has not precedents (Fig. 4). The presence of palladium was confirmed by Energy-dispersive X-ray Spectroscopy (EDS) measurements; sharp Pd Lα1 and Lβ1 peaks are clearly visible at 2.84 and 2.99 keV, respectively (Fig. 4c and Fig. 4f).

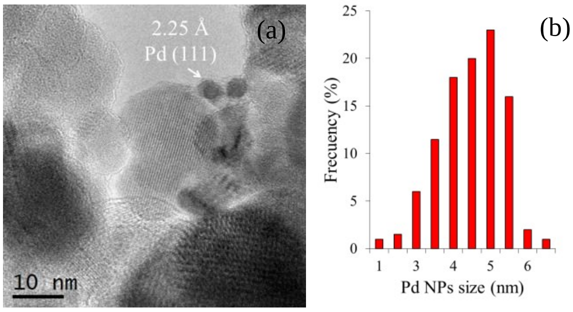

Fig. 2 (a) TEM images of Fe_3O_4dpa@$Pd_{1.0}$. (b) Histrogram of the Pd particle size distribution.

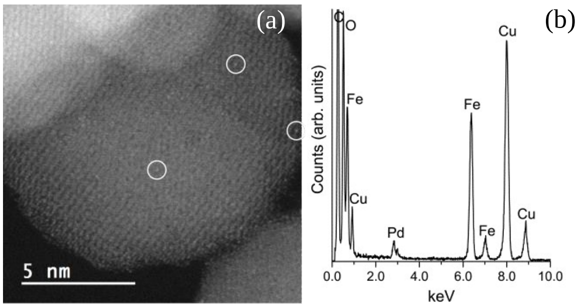

Fig. 3 (a) HAADF-STEM images of Fe_3O_4dpa@$Pd_{0.1}$. Isolated Pd atoms (white circles) are uniformly dispersed on the magnetite support. (b) EDS spectrum. The Cu and C signals originate from the TEM grid.

View Article Online
DOI: 10.1039/C6RA14257E

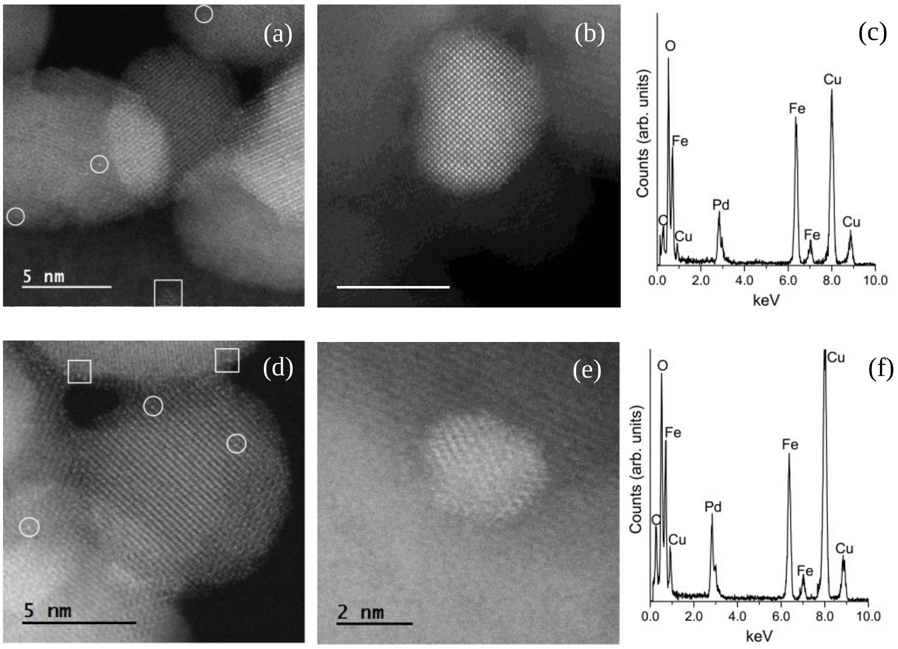

Fig. 4 (a,b) HAADF-STEM images of Fe_3O_4dpa@$Pd_{0.3}$ showing the presence of different Pd species. (c) EDS spectrum of Fe_3O_4dpa@$Pd_{0.3}$. (d,e) HAADF-STEM images of Fe_3O_4dpa@$Pd_{0.5}$ showing the presence of different Pd species. (f) EDS spectrum of Fe_3O_4dpa@$Pd_{0.5}$. The circles and squares in images indicate Pd single-atoms and clusters/nanoparticles, respectively.

X-ray Photoelectron Spectroscopy (XPS) was used to determine the surface elemental composition for Fe_3O_4dpa@Pd_x nanocomposites (Fig. S1). The surface Pd/Fe atomic ratios are compiled in Table 2. For the Fe_3O_4dpa@Pd_x catalysts with x=0.1, 0.3 and 0.5, the Pd/Fe ratio progressively increases from Pd/Fe=0.003 to 0.010 as expected since all the Pd single atoms and subnanometer clusters observed by HAADF-STEM are sampled. However, for the Fe_3O_4dpa@$Pd_{1.0}$ sample, the Pd/Fe ratio is lower because not all the Pd in the Pd nanoparticles is sampled given the larger dimensions of the Pd nanoparticles, in total accordance to high-resolution TEM results discussed above. The oxidation state of Pd in each catalyst is also included in Table 2, where the relative contributions from Pd(0), Pd(II) and Pd(IV) species and their binding energies (Pd $3d_{5/2}$) are indicated. There is a clear trend between the oxidation state of Pd and its content in the catalysts; the higher the Pd loading the more oxidized is Pd. The sample with the highest Pd content, Fe_3O_4dpa@$Pd_{1.0}$, exhibits photoemission peaks ascribed to Pd(IV), which confirms the tendency of Pd oxidation in this series. On the other hand, the sample Fe_3O_4dpa@$Pd_{0.1}$, which only contains Pd single atoms, exhibits a Pd(0) component at a significantly higher binding energy value (335.8 vs. 335.2-335.3 eV), which suggests that there is an electronic transfer from the Pd single atoms to the Fe_3O_4 support, in accordance to previous reports.[16,17]

Catalytic studies

Suzuki-Miyaura reaction. Palladium-catalyzed Suzuki-Miyaura cross-coupling is a well-known process for the synthesis of biaryls using aryl halides with arylboronic (Scheme 2) acids that have many applications in agrochemicals, natural products and pharmaceutical intermediates.[18] For testing the catalytic activity of Fe_3O_4dpa@Pd_x NPs the reaction between 4-bromobenzene and phenylboronic acid (1:1) was analysed and optimized in terms of time, temperature (Table S1), base (Table S2) and solvent (Table S3). The best results were obtained with Fe_3O_4dpa@$Pd_{0.5}$ NPs after 20 min at 65 °C in EtOH/water (1:1) and K_3PO_4. Table 3 lists the catalytic results. Note that Fe_3O_4dpa NPs in absence of Pd (entry 1) showed catalytic inactivity, while entry 2 revealed the poor catalytic behaviour of the NPs loaded with Pd in the absence of linker. Entries 3-6 display the results obtained with the rest of the Pd-containing NPs. Clearly, the best catalyst is the sample containing 0.5% of Pd (entry 5). The catalyst constituted only by single atoms (Fe_3O_4dpa@$Pd_{0.1}$) (entry 3) and the Fe_3O_4dpa @ $Pd_{0.3}$ (entry 4) are also excellent although the sample loaded with 1.0 Pd% is clearly less efficient (entry 6) due the large nanoparticles size.

We next proceeded to examine the scope and limitation of the catalysts. Working with Fe_3O_4dpa@$Pd_{0.5}$ NPs several bromo-aryl substrates were reacted with phenylboronic acid (1:1) and the coupling products were obtained in excellent yields (Table 4). Note that the Pd used is as low as 9.4×10^{-5} eq. To our knowledge the TOFs exhibited with Fe_3O_4 dpa@$Pd_{0.5}$ NPs for the Suzuki-Miyaura C-C coupling are by far the highest reported up to now.

Table 2 Pd/Fe surface atomic ratios, % of Pd species and binding energies obtained by XPS.

Catalyst	Pd/Fe	% (BE Pd $3d_{5/2}$, eV)		
		Pd(0)	Pd(II)	Pd(IV)
Fe_3O_4@Pd	0.006	42 (335.2)	58 (337.5)	-
Fe_3O_4dpa@$Pd_{0.1}$	0.003	48 (335.8)	52 (337.3)	-
Fe_3O_4dpa@$Pd_{0.3}$	0.005	30 (335.3)	70 (337.4)	-
Fe_3O_4dpa@$Pd_{0.5}$	0.010	18 (335.2)	82 (337.4)	-
Fe_3O_4dpa@$Pd_{1.0}$	0.007	18 (335.3)	58 (337.5)	24 (338.7)

View Article Online
DOI: 10.1039/C6RA14257E

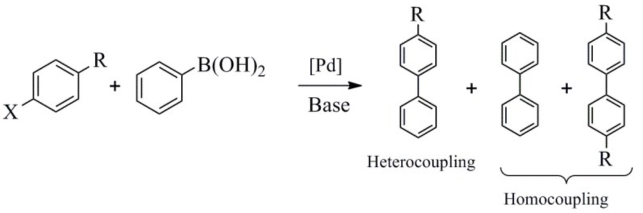

Scheme 2 Suzuki-Miyaura coupling.

Table 3 Activity of different catalyst in Suzuki-Miyaura coupling.

Entry	Catalyst	**TOF (h^{-1})**
1	Fe_3O_4dpa	0
2	Fe_3O_4@Pd	870
3	Fe_3O_4dpa@$Pd_{0.1}$	51200
4	Fe_3O_4dpa@$Pd_{0.3}$	64600
5	Fe_3O_4dpa@$Pd_{0.5}$	110000
6	Fe_3O_4dpa@$Pd_{1.0}$	1630

TOF (mol product/mol catalyst·time). Bromobencene (3 mmol), phenylboronic acid (3.6 mmol), K_3PO_4 (9 mmol), catalyst (9.4×10^{-5} mmol Pd), 65 °C, EtOH:water.

The lifetime of catalytic systems and their reusability is important for practical applications. The reusability of the catalyst was examined upon the reaction of bromobenzene and phenylboronic acid. In detail, the NPs were collected after completion of the first reaction by using an external magnet and washed with ethanol and dried. Then, the recovered catalyst nanoparticles were used for the next round by mixing them with a new substrate, base, and solvent. The third round was carried out following the same procedure and the results are displayed in Table 5. As can be seen, the loss of the catalytic efficiency is remarkably high and greater than that detected, for example, by employing Sdp linker.[12] The strong decrease of the catalytic activity is concomitant with the reduction of Pd concentration (33 wt%) found in the residual NPs. The measured leaching of Pd suggests that the catalytic process is essentially homogeneous, which was subsequently confirmed by a hot filtration test. Thus, bromobenzene with phenylboronic acid were reacted at 65°C. After 10 min. the solid catalyst was separated magnetically and the filtrate was transferred to another Schlenk flask. Without the presence of catalyst the reaction progressed to reach 95% of conversion after 30 min. This result is in good accord with recently reported data arguing that palladium species leached out from nanoparticles into the reaction mixture are indeed the actual catalytic species instead of the original Pd NPs.[19] In addition, the HAADF-STEM images of the catalyst after 3 cycles showed the presence of only palladium single atoms (Fig. 5) strengthening the idea that strong bonding between Pd single-atoms and naked Fe_3O_4 takes place.[16] This behavior explains the remaining activity of the catalyst after several cycles.

The Suzuki reaction with chloroaryl substrates is difficult to achieve. In this paper only traces of the final product have been observed by reaction of chlorobenzene and chlorotoluene with phenylboronic acid in the presence of Fe_3O_4dpa@$Pd_{0.5}$.

Table 4 Substrate effect on Suzuki-Miyaura coupling with Fe_3O_4dpa@$Pd_{0.5}$ as catalyst.

Bromoaryl	**TOF (h^{-1})**
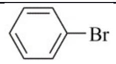	110 000
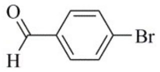	96 300
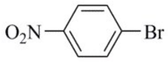	35 000
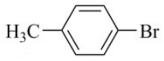	38 400
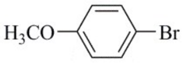	28 300

Bromoaryl (3 mmol), phenylboronic acid (3.6 mmol), K_3PO_4 (9 mmol), catalyst (9.4×10^{-5} mmol Pd), 65 °C, EtOH:water (60 mL).

Table 5 Reuse of Fe_3O_4dpa@$Pd_{0.5}$ as catalyst in the Suzuki-Miyaura coupling.

Cycle	**TOF (h^{-1})**
1	110000
2	19200
3	4800

Bromobencene (3 mmol), phenylboronic acid (3.6 mmol), K_3PO_4 (9 mmol), catalyst (9.4×10^{-5} mmol Pd), 65 °C, EtOH:water 1:1.

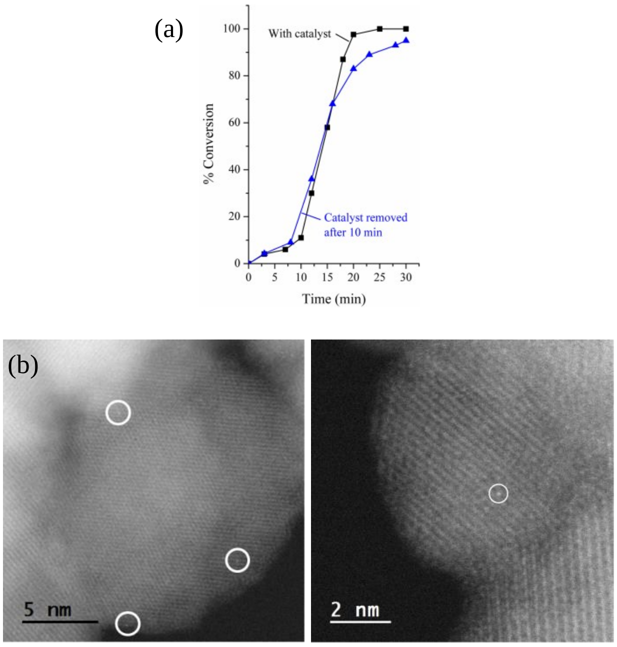

Fig. 5 (a) Conversion of 4-bromobencene after Fe_3O_4dpa@$Pd_{0.5}$ removal. (b) HAADF-STEM of Fe_3O_4dpa@$Pd_{0.5}$ after the third recycling process. Only Pd single-atoms were present (white circles).

View Article Online
DOI: 10.1039/C6RA14257E

Catalysis in neat water. There are only very few articles on the application of magnetically separable Pd-catalyzed Suzuki-Miyaura reaction in neat water, and in some of the examples the process required the use of large amounts of ionic liquids or phase transfer reagents.[20] That is, there is still much room for developing new magnetically recoverable catalyst in pure water. Here, we report the catalytic behaviour of Fe_3O_4dpa@$Pd_{0.5}$ NPs in water for the Suzuki coupling under atmosphere. Although the boronic acids are soluble in water, the efficiency of Suzuki reaction in neat water can be affected by side reactions, mainly, homocoupling reactions of the boronic acids. The reaction of 4-bromobenzene and phenyl boronic acid was used as model reaction and optimized in terms of time and temperature. We next examined the scope of this process using several substrates (Table 6). It is well-known that the coupling reactions of aryl bromides containing electron–donating groups proceeded more efficiently than those having electron-withdrawing groups. This trend is not observed in our results because the solubility of the substrates is the predominant factor in water. Formation of homocoupling products was negligible. The overall results shown in Table 7 are exceptional in terms of TOFs and selectivity overcoming all those reported earlier, but the reusability is very limited. For example, using bromobenzaldehyde as a reagent it was found that after the third cycle the TOF decreased from 5030 to 106 h^{-1}. Palladium leaching was clearly evidenced by a hot filtration test in which the important loss (28 wt%) of Pd content (by ICPoes analysis) in residual NPs confirmed the homogeneous nature of the catalytic process.

Table 6 Suzuki-Miyaura coupling with different substrates using Fe_3O_4dpa@$Pd_{0.5}$ as catalyst.

Bromoaryl	TOF (h^{-1})
	3150
	5030
	0
	1479
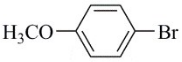	475

Bromoaryl (0.5 mmol), phenylboronic acid (0.6 mmol), K_3PO_4 (1.5 mmol), 2.0×10^{-4} mmol Pd, 65 °C, water, air atmosphere.

Table 7 Comparison of Suzuki-Miyaura coupling catalyzed by Pd NPs from the literature.

Support	Substrate	Solvent	Base	Temperature (°C)	TOF(h^{-1})	Ref.
Fe_3O_4dpa@$Pd_{0.5}$	BB	EtOH:H_2O	K_3PO_4	65	110000	This work
Fe_3O_4dpa@$Pd_{0.5}$	BB	H_2O	K_3PO_4	65	1470	This work
Fe_3O_4Sdp@$Pd_{0.5}$	4-BA	EtOH:H_2O	KOH	65	60	12
γ-Fe_2O_3/dendrimer	4-BN	THF/Triton	NaOH	65	41.7	21
Fe_3O_4-SiO_2/phosphine	4-BN	H_2O /DMF	K_2CO_3	25	13.1	22
Fe_3O_4-SiO_2/phosphine-Pd(II)	4-BA	MeOH	K_3PO_4	60	132	23
Graphitic carbon nitride/none	4-BN	EtOH:H_2O	KOH	25	232	24
None support/ionic phosphine	4-BA	Glycerol	*t*-BuOK	100	50	25
Fe_3O_4-SiO_2/iminophosphine	4-BA	Toluene	KOH	100	100	11b
Fe_3O_4/dopamine-phosphine	4-BA	Toluene	KOH	100	33	11a
$NiFe_2O_4$/dopamine	4-BA	DMF	K_3PO_4	65	0.4	26
Carbon	4-BA	EtOH:H_2O	NaOH	65	171	24
Phosphine dendrimer	4-BD	Dioxane	K_3PO_4	100	82.5	27
Fe_3O_4	4-BA	Toluene	Na_2CO_3	130	0.01	28
Click dendrimer	BB	EtOH: H_2O	K_3PO_4	28	16500	29
Fe_3O_4-SiO_2/ TEG-imidazolium	BB	H_2O	K_2CO_3	60	437	30
Multi-walled carbon nanotubes/Pd/PdO	BB	H_2O	*i*-Pr_2NH	100	250	31
Fe_3O_4/Triazole-acid	BB	EtOH: H_2O	K_2CO_3	70	2920	32

4-BN: 4-bromonitrobenzene. 4-BA: 4-bromoanisol. BB, bromobencene.

Hydrogenation of 4-nitrophenol. Nitrophenol is a by-product produced from pesticides and synthetic dyes that causes damage to central nervous human system so that its removal from the environment is a crucial task.[33] Recently, FeO_x-supported platinum SAC[34] and carbon nitride- palladium SAC[35] have been reported to show excellent activity for the hydrogenation of nitroarenes but, to our knowledge, the Pd SACs supported on magnetite NPs have not

View Article Online
DOI: 10.1039/C6RA14257E

explored for the reduction of 4-nitrophenol in water.

The aqueous phase reduction reaction of 4-nitrophenol (4-NP) to 4-aminophenol (4-AP) (Scheme 3) using metal-supported NPs is a model reaction that permits to compare the efficiency of the catalysts employed. Esumi *et al* have proposed that the catalytic reduction of 4-NP proceeds in two steps: i) diffusion and adsorption of 4-NP to the catalyst surface and ii) electron transfer mediated by the catalyst surface from BH_4^- to 4-NP.[36] The rapid reduction generally is carried out using $NaBH_4$ and monitored by time-resolved UV/Visible spectra. We have tested this reaction with the catalysts Fe_3O_4dpa@Pd_x NPs and the results are listed in Table 8. The TOFs measured are also very high, including that obtained with a sample having Pd deposited on their magnetite surface without the assistance of dpa (entry 1). In all cases the reaction takes place with rapid release of H_2 bubbles accompanied with a decrease of the absorption at 400 nm and the appearance of other at 317 nm, confirming the transformation of 4-nitrophenol to 4-aminophenol (Fig. 6a). The UV-Vis spectra showed an isosbestic point (313 nm) indicating that no by-product is formed during the reduction of 4-NP. Since the concentration of $NaBH_4$ exceeds that of 4-nitrophenol ($c(NaBH_4)/c(\text{nitrophenol})$ = 100:1) the reduction can be considered as pseudo-first-order reaction with regard to 4-nitrophenol only. The plot matches the first-order reaction kinetics and the rate constant is calculated from the equation $ln(c_t/c_o)=kt$. Figure 6b shows the linear relationship between $ln(c_t/c_0)$ and the reaction time for Fe_3O_4dpa@$Pd_{0.3}$. For a quantitative comparison, we have introduced the activity parameter $k' = k(s^{-1})/m_{Pd}$ where m_{Pd} is the total mass of the palladium added as catalyst. From the catalytic results (Table 8) it can be seen that the best sample is Fe_3O_4dpa@$Pd_{0.1}$ that contains only 0.10% of palladium. As commented above this catalyst is constituted by Pd SACs, which enormous catalytic activity has been recently recognized in different reactions.

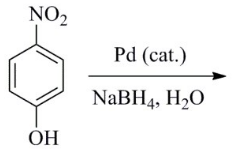

Scheme 3 Reduction of 4-NP.

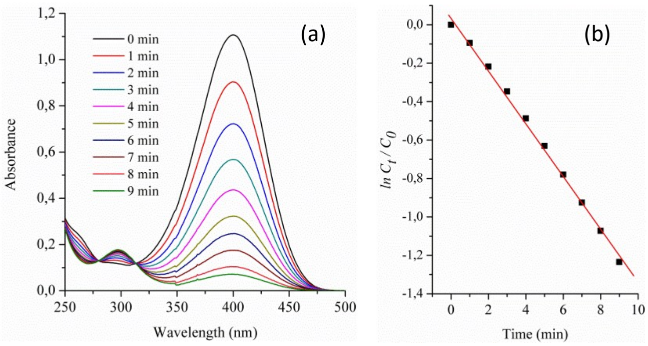

Fig. 6 Catalytic reduction of 4-nitrophenol (4-NP) to 4-aminophenol (4-AP) with Fe_3O_4dpa@$Pd_{0.3}$. (a) UV-Vis spectra of time dependent reaction. (b) ln C_t / C_0 vs. time of reaction.

Table 8 Activity of catalysts in 4-NP reduction.

Catalyst	$k'(s^{-1}g^{-1})$
Fe_3O_4@Pd	24500
Fe_3O_4dpa@$Pd_{0.1}$	90000
Fe_3O_4dpa@$Pd_{0.3}$	58000
Fe_3O_4dpa@$Pd_{0.5}$	50600
Fe_3O_4dpa@$Pd_{1.0}$	16300

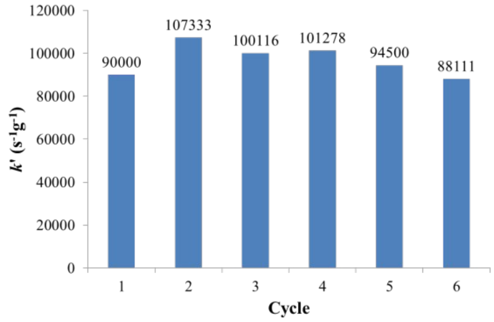

Fig. 7 Activity of Fe_3O_4dpa@$Pd_{0.1}$ per cycle in 4-NP reduction.

Table 9 Comparison of reduction of 4-NP catalyzed by Pd NPs from the literature.

Catalyst	k (s^{-1})	k' ($s^{-1}g^{-1}$)	Ref.
Fe_3O_4dpa@$Pd_{0.1}$	$3.6×10^{-3}$	107333	This work
rGO/Pd–Fe_3O_4/PPy	$3.2×10^{-3}$	152153	37
MOF	$1.2×10^{-2}$	7827	38
[Fe_3O_4Sdp@Pd]$_{OX}$	$4.4×10^{-2}$	6100	12
PdNPs/Fe_3O_4/dopamine-phosphine	$2.0×10^{-2}$	2349	11a
PdNPs /Fe_3O_4-Ag core-shell	$3.3×10^{-2}$	1736	39
PdNPs/Polypirrol capsule	$8.9×10^{-3}$	1415	40
PdNPs/Fibrous nano-silica	$8.0×10^{-3}$	1026	41
PdNPs/Mesoporous silica	$1.2×10^{-2}$	750	42
Pd-AuNPs/graphene	$6.5×10^{-3}$	130	43

Table 9 permits to compare the efficiency of a good number of catalytic species and it can be seen that the efficiency of the Fe_3O_4dpa@$Pd_{0.1}$ NPs overcomes largely the majority of them. The reusability of the catalysts has been examined. The catalytic efficiency is maintained during the first six cycles for Fe_3O_4dpa@$Pd_{0.1}$ (Fig. 7). Then, it began to drop. ICPoes analysis indicated that the Pd content of the resulting NPs after six cycles decreased only 6%. This fact along with the constant activity shown for the catalyst through the cycles seems to indicate that reduction of nitrophenol occurs heterogeneously.

Hydrogenation of styrene. Very recently, we have described the catalytic activity of Fe_3O_4dopPPh_2@Pd_x NPs supported on magnetite nanoparticles using styrene hydrogenation as a model catalytic reaction in isopropanol as solvent at room temperature in a hydrogen atmosphere.[17] Surprisingly we observed that a sample containing a very low Pd weight content (0.18wt%) and constituted uniquely by Pd SACs was absolutely inactive for the hydrogenation of styrene and other alkenes. This is the first time that Pd single

View Article Online
DOI: 10.1039/C6RA14257E

atom catalyst (SACs) were shown to be catalytically inactive. In contrast, samples with higher Pd content, exhibiting small clusters and nanoparticles, gave exceptional catalytic results. These findings prompted us to analyse the catalytic activity of Fe_3O_4dpa@Pd_x NPs for the hydrogenation of styrene in order to check whether our catalysts are able to mimic the catalytic behaviour shown by the Fe_3O_4dopPPh_2@Pd_x NPs. The results are compiled in Table 10. The most remarkable result was the null activity shown by sample Fe_3O_4dpa@$Pd_{0.1}$ NPs (entry 2). This result confirms the no-activity of Pd SACs for the hydrogenation of styrene and it is opposed to the excellent catalytic efficiency reported in a number of processes.[44] Significantly, the rest of samples followed the expected catalytic trend, that is, excellent performances that deteriorate with the increase of Pd content and size of the Pd nanoparticles.

Reusability studies have been carried out on the best catalytic sample Fe_3O_4dpa@$Pd_{0.5}$. The loss of activity is very small (Table 11) which is confirmed by the final Pd content after 3 rounds, less than 3% in relation to the starting sample. These results strongly support the catalytic heterogeneous behaviour for this process. In Table 12 are listed selected catalysts for hydrogenation of styrene including reaction conditions and TOFs where the Pd catalysts reported here are among the best ones.

Conclusions

In conclusion, in this work we demonstrate that the use of the dpa molecule as a linker for the deposition of palladium species on the magnetite surface has permitted to solubilize partially the resulting hybrid in water. This fact along with the partial removal of dpa during the reduction process facilitates the approach of the substrates to the catalyst. In addition to this, the small size of the Pd NPs supported on the magnetite in Fe_3O_4dba@$Pd_{0.3}$ and Fe_3O_4dba@$Pd_{0.5}$ along with the presence of Pd SACs, explains the exceptional results for the Suzuki C-C coupling reaction and hydrogenation of 4-nitrophenol both in neat water and in a mixture of ethanol/water.

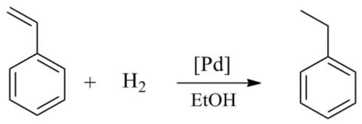

Scheme 4 Styrene hydrogenation.

Table 10 Activity of the catalyst in styrene hydrogenation.

Entry	Catalyst	TOF (h^{-1})
1	Fe_3O_4@Pd	404
2	Fe_3O_4dpa@$Pd_{0.1}$	0
3	Fe_3O_4dba@$Pd_{0.3}$	4690
4	Fe_3O_4dba@$Pd_{0.5}$	4880
5	Fe_3O_4dba@$Pd_{1.0}$	3630

3 bar H_2, 5 mmol styrene, 25 °C, EtOH, 1h.

Table 11 Styrene hydrogenation per cycle with Fe_3O_4dpa@$Pd_{0.5}$ as catalyst.

Cycle	TOF (h^{-1})
1	4880
2	4793
3	4760

3 bar H_2, 5 mmol styrene, 25 °C, EtOH.

Table 12 Comparison of styrene hydrogenation catalyzed by Pd NPs from the literature.

Catalyst	Solvent	Pressure (bar)	T (°C)	TOF (h^{-1})	Ref.
Fe_3O_4dpa@$Pd_{0.5}$	EtOH	3	25	4880	This work
$[Fe_3O_4Sdp@Pd]_{ox}$	EtOH	3	25	3100	12
Polivinilpiridina/$PdCl_2$	EtOH	1	25	6944	45
PdNPs/Polietilenglicol	EtOH	3	25	660	46
Polyestyrene/Pd complex	DMF	1	25	766	47
PdNPs/Stearate/Oleyl amine	Cyclohexane	21	50	7704	48
MOF/Pd	None	1	35	703	49
Pd/C	Ethyl acetate	3	25	163	50

Acknowledgements

This work was financially supported by the MICINN (projects CTQ2012-31335 and CTQ2015-65040-P). J. L. is a Serra Húnter Fellow and is grateful to the ICREA Academia program. Access to the TEM facilities at IBM Research-Zurich, Switzerland, under the IBM/Empa Master Joint Development Agreement is gratefully acknowledged. A. G. thanks University of Tolima (Colombia) for financial support.

Experimental

All manipulations were performed under purified nitrogen using standard Schlenk Techniques. Organic Elemental Analysis (OEA) was performed in an Elemental Analyzer Thermo Scientific Flash 2000 A7 model. The Infrared Spectrum (IR) was plot with a NICOLET Impact 400 FT-IR. And the abbreviations used for signals were: w (weak), m (medium), s (strong), only significant signals are mentioned. Thermogravimetric Analysis (TGA) was performed on IGA 851 Mettler-Toledo instrument, nitrogen flow (50 mL/min), from 30 up to 1000 °C, and 10 °C/min as gradient. ICPoes (Inductively Coupled Plasma optical emission spectrometry) analysis was achieved in a Perkin Elmer 3200RL model. Samples were dissolved in HCl/HNO_3 3:1 (v/v) mixture. High-angle annular dark-field scanning transmission electron microscopy (HAADF-STEM) and energy-dispersive X-ray spectroscopy (EDS) were carried out using a double spherical aberration-corrected JEOL JEM-ARM200F microscope operated at 200 kV, and equipped with a JEOL Dry SD100GV silicon drift detector with 100 mm^2 detection area for EDS analysis. The microscope was setup in STEM mode with a probe semiconvergence angle set to 25.3 mrad which yields a calculated probe size of about 80 pm. The annular semidetection range of the annular dark-field detector was set to collect electrons scattered between 90 and 370 mrad. Transmission electron microscopy (TEM) images were registered at 200 kV in a JEOL 2010F instrument having a point resolution of 0.21 nm. Samples were prepared by placing a drop of solution on a holey-carbon-coated Cu TEM grid and allowing the solvent to evaporate in air. In addition, for the HAADF-STEM experiments, the samples were gently plasma cleaned with an Ar (75%) / O_2 (25%) plasma for a few seconds to remove hydrocarbon contamination from the surfaces of the nanoparticles. XPS (X-ray Photoelectron Spectroscopy) analysis was carried out in a SPECS instrument with Al X-ray source and a Phoibos 150 analyzer. The spectrum was recorded under 10^{-7} Pa. Binding energies were referred to the C 1s signal at 284.8 eV. All reactants were purchased from suppliers in “for synthesis” quality or higher and used without further purification. The solvents were HPLC quality and/or were dried trough *pure solve* instrument from Innovate Tehcnology USA Inc. Deionized water was obtained from Milipore Helix 3 water purification system.

Synthesis of ferrite nanoparticles (Fe_3O_4). 6.95 g (25.3 mmol) of iron(II) sulphate heptahydrate was mixed with 10.0 g of iron(III) sulphate hydrate and dissolved in water (250 mL). Then an ammonia 25 % solution was slowly added to adjust pH up to 10. The reaction mixture was stirred for 1 h at 50 °C. The nanoparticles obtained were separated magnetically and washed with water until pH 7 was attained. The resulting nanoparticles were dried under reduced pressure at 60 °C for 2 h.

Synthesis of Fe_3O_4@Pd. 100 mg of magnetite nanoparticles were sonicated in methanol (10 ml) for 30 min. Then, 4.1 mg (12.5 µmol) of $K_2[PdCl_4]$ dissolved in water (2 mL) were added and stirred (1000 rpm) for 2 h. After that, the nanoparticles were washed with water (3 × 10 mL), acetone (10 mL), and water (10 mL). Next, the NPs were dispersed in water (8 mL) and an aqueous solution (2.5 mL) of sodium borohydride 0.05 M was added. Then, the nanoparticles were washed with water (3 × 30 mL) and acetone, removed by an external magnet and dried under reduced pressure. ICPoes: 0.68 % Pd.

Synthesis of Fe_3O_4dpa. 400 mg of ferrite nanoparticles were sonicated in ethanol (15 mL) for 30 min. Then, a solution of 4-(diphenylphosphino)benzoic acid (dpa, 306 mg, 1 mmol) in methanol (15 mL) was added to the suspended Fe_3O_4. This mixture was sonicated for 2 h and the resulting nanoparticles were washed with ethanol (3 × 30 mL) and acetone (30 mL). Finally, the Fe_3O_4dpa nanoparticles were collected by magnetic separation and dried under reduced pressure. OEA: 2.4 %C, 3.2% dpa.

Synthesis of Fe_3O_4dpa@Pd_x (x = 1, 0.5, 0.3, 0.1). 400 mg of **Fe_3O_4dpa** were dispersed in water (40 mL) for 10 min by sonication. Next, a quantity (depending on *x;* 50 µmol, 25 µmol, 12 µmol, 4 µmol, respectively) of $K_2[PdCl_4]$ dissolved in water (8 mL) were added and stirred (1000 rpm) for 2 h. After that, the nanoparticles were washed with water (1 x 50 mL), ethanol (2 × 50 mL) and acetone (50 mL), and dried under reduced pressure. Next, 400 mg of these nanoparticles were dispersed in water (40 mL) by sonication and 10 mL of an aqueous solution of sodium borohydride 0.05 M was added. The mixture was stirred (1200 rpm) for 2 h. Then, the nanoparticles were washed with water (1 × 50 mL), ethanol (2 × 50 mL) and acetone (50 mL), removed by an external magnet and dried under reduced pressure. ICPoes: 1.1%, 0.50%, 0.32%, and 0.097% of palladium for Fe_3O_4dpa@Pd_x, where x = 1, 0.5, 0.3, and 0.1, respectively).

View Article Online
DOI:10.1039/C6RA14257E

Suzuki-Miyaura coupling. In a typical Suzuki-Miyaura reaction 3.6 mmol of phenylboronic acid, 9 mmol of base, and a quantity of Pd catalyst (e.g. 2.0 mg of Fe_3O_4Sdp@$Pd_{0.5}$, 9.4×10^{-5} mmol) were weighed into a Schlenk tube. The mixture was purged with nitrogen and 60 mL of solvent was added. After that, the tube was brought to a preheated plate at 65 °C, and 3 mmol (1 eq) of substrate was added. When the desirable reaction time was reached, the mixture was allowed to cool down. An extraction with ethyl acetate was needed. The organic phase was removed, dried over sodium sulphate and analyzed by GC. The identity of products was confirmed by GC-MS analysis.

Catalytic reduction of *p*-nitrophenol. 30 µL of *p*-nitrophenol (7.4 mM) and 30 µL of $NaBH_4$ (0.40 M) were added into a quartz cuvette containing 2 mL of water. Then, 30 µL of an aqueous suspension containing the catalyst nanocomposite (3 to 5 mg approximately in 5 mL of water) was injected into the cuvette to start the reaction. The intensity of the absorption peak at 400 nm in UV-Vis spectroscopy was used to monitor the process of the conversion of *p*-nitrophenol to *p*-aminophenol. After each cycle of reaction, another 30 µL of *p*-nitrophenol and 30 µL of $NaBH_4$ were added to the reaction to study the reuse of the catalyst. The catalytic reduction reactions were conducted at room temperature.

Hydrogenation of styrene. Hydrogenation reactions were carried out in a hydrogen atmosphere at room temperature. Typically, under nitrogen, ferrite catalyst (5.0 mg approximately) was dispersed in ethanol freshly distilled (20 mL), and then, styrene (2.5 mmol) was poured. After that, the mixture was transfer into a Fisher-Porter reactor, filled with hydrogen (3 bar), and stirred at constant speed. The conversion was determined by GC analysis.

References

1 a) M. Lamblin, L. Nassar-Hardy, J.C. Hierso, E. Fouquet and F. X. Felpin, *Adv. Synth. Catal*. 2010, **352**, 33-79; b) S. Paul, M. M. Islam and Sk. M. Islam, *RSC Adv*. 2015, **5**, 42193-42221.

2 F. Lu, J. Ruiz, D. Astruc, *Tetrahedron Lett.* 2004, **45**, 9443-9445.

3 A. Balanta, C. Godard, C. Claver, *Chem. Soc. Rev.* 2011, **40**, 4973- 4985.

4 R. M. Crooks, M. Zhao, L. Sun, V. Chechik, L. K. Yeung, *Acc. Chem. Res.* 2000, **34**, 181-190.

5 V. K. R. Kumar, K. R. Gopidas, *Tetrahedron Lett.*, 2011, **52**, 3102-3105.

6 E. Raluy, I. Favier, A. M. López-Vinasco, C. Pradel, E. Martin, D. Madec, E. Teuma, M. Gómez, *Phys. Chem. Chem. Phys.* 2011, **13**, 13579-13584.

7 P. Sonström, M. Bäumer, *Phys. Chem. Chem. Phys.* 2011, **13**, 19270-19284.

8 a) D. Wang and D. Astruc, *Chem. Rev*. 2014, **114**, 6949-6985; b) R. B. N. Baig and R. S. Varma, *Chem. Commun*. 2013, **49**, 752-770; c) W. Dong and D. Astruc, *Molecules* 2014, **19**, 4635-4653; d) W. Dong, C. Deraedt, L. Salmo, C. Labrugere, L. Etienne, J. Ruiz and D. Astruc, *Chem. Eur. J.* 2014, **21***,* 6501-6512; e) L. M. Rossi, N. J. S. Costa, F. P. Silva and R. Wojcieszak, *Green Chem***.** 2014, **16***,* 2906-2933; e) M. B. Gawande, P. S. Branco and R. S. Varma, *Chem. Soc. Rev*. 2013, **42**, 3371-3393; f) S. Roy and M. A. Pericàs, *Org. Biomol. Chem*. 2009, **7**, 2669-2677.

9 a) R. Polshettivar, R. Luque, A. Fihri, H. Zhu, M. Bouhra and J. M. Basset, *Chem. Rev*. 2011, **111**, 3036-3075; b) V. Polshettiwar and R. S. Varma, *Green Chem*. 2010, **12**, 743-754; c) R. B. N. Baig and R. S. Varma, *Chem. Commun*. 2012, **48**, 2582-2584; d) R. B. N. Baig and R. S. Varma, *Green Chem*. 2013, **15**, 398-417.

10 a) K. Jiang, H-X Zhang, Y-Y. Yang, R. Mothes, H. Lang and W-B Cai, *Chem. Commun.* 2011, **43**, 11924-11926; b) P. Li, L. Wang, L. Zhang and G-W Wang, *Adv. Synth. Catal*. 2012, **354**, 1307-1318.

11 a) F. Gonzàlez de Rivera, I. Angurell, M. D. Rossell, R. Erni, J. Llorca, N. J. Divins, G. Muller, M. Seco and O. Rossell, *Chem. Eur. J.* 2013, **19**, 11963-11974; b) N. J. S. Costa, P. K. Kiyohara, A. L. Monteiro, Y. Coppel, K. Philippot and L. M. Rossi, *J. Catal*. 2010, **276**, 382-389.

12 A. Guarnizo, I. Angurell, M. D: Rossell, J. Llorca, G. Muller, M. Seco and O. Rossell, *RSC Adv*. 2015, **5**, 91340-91348.

13 J. M. Thomas, *Nature*, 2015, **525**, 325–6.

14 V. Polshettiwar and R. S. Varma, *Chem. Eur. J.* 2009, **15**, 1582-1586.

15 X.-F. Yang, A. Wang, B. Qiao, J. Li, J. Liu and T. Zhang, *Acc. Chem. Res.*, 2013, **46**, 1740–8.

16 G. S. Parkinson, Z. Novotny, G. Argentero, M. Schmid, J. Pavelec, R. Kosak, P. Blaha and U. Diebold, *Nat. Mater.*, 2013, **12**, 724–8.

17 M. D. Rossell, F. J. Caparrós, I. Angurell, G. Muller, J. Llorca, M. Seco, O. Rossell, *Catal. Sci. Technol*. 2016, **6**, 4081-4086.

18 a) N. Miyaura and A. Suzuki, *Chem. Rev*. 1995, **95**, 2457-2483; b) M. Moreno-Mañas and R. Pleixats, *Acc. Chem. Res*. 2003, **36**, 638-643; c) A. Suzuki and Y. Yamamoto, *Chem. Lett*. 2011, 40, 894-901; d) A. Balanta, C. Godard and C. Claver, *Chem. Soc. Rev*., 2011, **40**,4973-4985.

19 A. Bej, K. Ghosh, A. Sarkar and D. W. Knight, *RSC Adv*. 2016, **6**, 11446-11453.

20 a) M. J. Jin and D. H. Lee, *Angew. Chem. Int. Ed*., 2010, **49**, 1119-1122; b) A. Taher, J. B. Kim, J. Y. Jun, W. S. Ahn and M. J. Jin, *Synlett*, 2009, 2477-2482; c) Z. Yinghuai, S. C. Peng, A. Emi, S. Zhenshun, M. Lisa and R. A. Kemp, *Adv. Synth. Catal*., 2007, **349**, 1917-1922; d) B. Karimi, F. Mansouri and H. Vali, *Green Chem*., 2014, **16**, 2587-2596.

21 D. Rosario-Amorin, X. Wang, M. Gaboyard, R. Clérac, S. Nlate and K. Heuzé, *Chemistry*, 2009, **15**, 12636–43.

22 Q. Du, W. Zhang, H. Ma, J. Zheng, B. Zhou and Y. Li, *Tetrahedron*, 2012, **68**, 3577–3584.

23 P. Li, L. Wang, L. Zhang and G.-W. Wang, *Adv. Synth. Catal.*, 2012, **354**, 1307–1318.

24 J. Sun, Y. Fu, G. He, X. Sun and X. Wang, *Appl. Catal. B Environ.*, 2015, **165**, 661–667.

25 F. Chahdoura, I. Favier, C. Pradel, S. Mallet-Ladeira and M. Gómez, *Catal. Commun.*, 2015, **63**, 47–51.

26 D. Guin, B. Baruwati and S. V Manorama, *Org. Lett.*, 2007, **9**, 1419–21.

27 L. Wu, B.-L. Li, Y.-Y. Huang, H.-F. Zhou, Y.-M. He and Q.-H. Fan, *Org. Lett.*, 2006, **8**, 3605–8.

28 R. Cano, D. J. Ramón and M. Yus, *Tetrahedron*, 2011, **67**, 5432–5436.

29 C. Deraedt, L. Salmon, L. Etienne, J. Ruiz and D. Astruc, *Chem. Commun. (Camb).*, 2013, **49**, 8169–71.

30 B. Karimi, F. Mansouri and H. Vali, *Green Chem.*, 2014, **16**, 2587-2596.

31 F. Yang, C. Chi, S. Dong, C. Wang, X. Jia, L. Ren, Y. Zhang, L. Zhang and Y. Li, *Catal. Today*, 2015, **256**, 186–192.

32 S. Su, G. Yue, D. Huang, G. Yang, X. Lai and P. Zhao, *RSC Adv.*, 2015, **5**, 44018–44021.

33 T. Aditya, A. Pal and T. Pal, *Chem. Commun*. 2015, **51**, 9410-9431.

34 H. Wei, X. Liu, A. Wang, L. Zhang, B. Qiao, X. Yang, Y. Huang, S. Miao, J. Liu and T. Zhang, *Nat. Commun.*, 2014, **5**, 5634.

35 G. Vilé, D. Albani, M. Nachtegaal, Z. Chen, D. Dontsova, M. Antonietti, N. Lopez and J. Perez-Ramirez, *Angew. Chem., Int. Ed.*, 2015, **54**, 11265-11269.

36 K. Hayakawa, T. Yoshimura and K. Esumi, *Langmuir*, 2003, **19**, 5517-5521.

37 T. Yao, H. Wang, Q. Zuo, J. Wu, X. Zhang, F. Cui and T. Cui, *Chem. Asian J.*, 2015, **10**, 1940–7.

38 Z. Dong, X. Le, Y. Liu, C. Dong and J. Ma, *J. Mater. Chem. A*, 2014, **2**, 18775–18785.

39 K. Jiang, H.-X. Zhang, Y.-Y. Yang, R. Mothes, H. Lang and W.-B. Cai, *Chem. Commun. (Camb)*, 2011, **47**, 11924–6.

40 Y. Xue, X. Lu, X. Bian, J. Lei and C. Wang, *J. Colloid Interface Sci.*, 2012, **379**, 89–93.

41 X. Le, Z. Dong, X. Li, W. Zhang, M. Le and J. Ma, *Catal. Commun.*, 2015, **59**, 21–25.

42 J. Morère, M. J. Tenorio, M. J. Torralvo, C. Pando, J. A. R. Renuncio and A. Cabañas, *J. Supercrit. Fluids*, 2011, **56**, 213–222.

43 C.-H. Liu, R.-H. Liu, Q.-J. Sun, J.-B. Chang, X. Gao, Y. Liu, S.-T. Lee, Z.-H. Kang and S.-D. Wang, *Nanoscale*, 2015, **7**, 6356–62.

44 a) E. J. Peterson, A. T. De La Riva, S. Lin, R. S. Johnson, H. Guo, J. T. Miller, J. H. Kwak, C. H. F. Peden, B. Kiefer, L. F. Allard, F. H. Ribeiro and A. K. Datye, *Nat. Commun.*, 2014, **5**, 4885; b) S. F. J. Hackett, R. M. Brydson, M. H. Gass, I. Harvey, A. D. Newman, K. Wilson and A. F. Lee, *Angew. Chem., Int. Ed.*, 2007, **46**, 8593-8596; d) H. Yan, H. Cheng, H. Yi, Y. Lin, T. Yao, C. Wang, J. Li, S. Wei and J. Lu, *J. Am. Chem. Soc.*, 2015, **137**, 10484-10487; e) G. Kyriakou, M. B. Boucher, A. D. Jewell, E. A. Lewis, T. J. Lawton, A. E. Baber, H. L. Tierney, M. Flytzani-Stephanopoulos and E. C. H. Sykes, *Science (Washington, DC, U. S.)*, 2012, **335**, 1209-1212.

45 S. Gao, W. Li and R. Cao, *J. Colloid Interface Sci.*, 2015, **441**, 85–9.

46 F. A. Harraz, S. E. El-Hout, H. M. Killa and I. A. Ibrahim, *J. Catal.*, 2012, **286**, 184–192.

47 S. M. Islam, A. S. Roy, P. Mondal and N. Salam, *Appl. Organomet. Chem.*, 2012, **26**, 625–634.

48 C. H. Yen, H.-H. Wei, H.-W. Lin and C.-S. Tan, *Appl. Organomet. Chem.*, 2012, **26**, 736–742.

49 Y. Pan, D. Ma, H. Liu, H. Wu, D. He and Y. Li, *J. Mater. Chem.*, 2012, **22**, 10834-10839.

50 C.-B. Hwang, Y.-S. Fu, Y.-L. Lu, S.-W. Jang, P.-T. Chou, C. R. C. Wang and S. J. Yu, *J. Catal.*, 2000, **195**, 336–341.

View Article Online
DOI: 10.1039/C6RA14257E

The linker dpa allows to deposit palladium on magnetite nanoparticles that show excellent catalytic behavior in water or water/ethanol solvents.

View Article Online
DOI: 10.1039/C6RA14257E

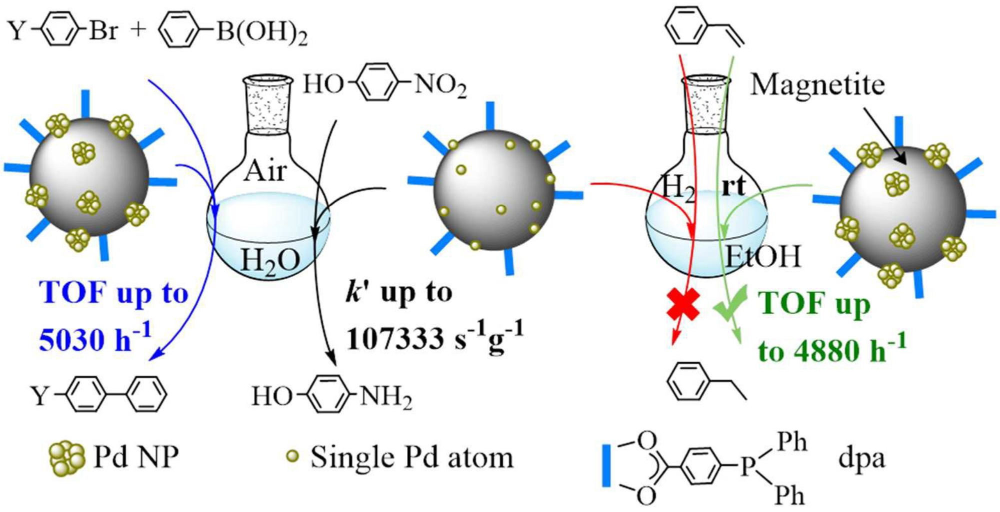

168x85mm (150 x 150 DPI)